Structure of the Complex of Calmodulin with the Target Sequence of Calmodulin-Dependent Protein Kinase I: Studies of the Kinase Activation Mechanism‡

Julie A. Clapperton,[§,||] Stephen R. Martin,[||,⊥] Stephen J. Smerdon,[§] Steven J. Gamblin,*[,§] and Peter M. Bayley[⊥]

Division of Protein Structure and Division of Physical Biochemistry, National Institute for Medical Research, Mill Hill, London NW7 1AA, U.K.

Received August 16, 2002; Revised Manuscript Received October 9, 2002

ABSTRACT: Calcium-saturated calmodulin (CaM) directly activates CaM-dependent protein kinase I (CaMKI) by binding to a region in the C-terminal regulatory sequence of the enzyme to relieve autoinhibition. The structure of CaM in a high-affinity complex with a 25-residue peptide of CaMKI (residues 294−318) has been determined by X-ray crystallography at 1.7 Å resolution. Upon complex formation, the CaMKI peptide adopts an α-helical conformation, while changes in the CaM domain linker enable both its N- and C-domains to wrap around the peptide helix. Target peptide residues Trp-303 (interacting with the CaM C-domain) and Met-316 (with the CaM N-domain) define the mode of binding as 1−14. In addition, two basic patches on the peptide form complementary charge interactions with CaM. The CaM−peptide affinity is ∼1 pM, compared with 30 nM for the CaM−kinase complex, indicating that activation of autoinhibited CaMKI by CaM requires a costly energetic disruption of the interactions between the CaM-binding sequence and the rest of the enzyme. We present biochemical and structural evidence indicating the involvement of both CaM domains in the activation process: while the C-domain exhibits tight binding toward the regulatory sequence, the N-domain is necessary for activation. Our crystal structure also enables us to identify the full CaM-binding sequence. Residues Lys-296 and Phe-298 from the target peptide interact directly with CaM, demonstrating overlap between the autoinhibitory and CaM-binding sequences. Thus, the kinase activation mechanism involves the binding of CaM to residues associated with the inhibitory pseudosubstrate sequence.

Changes in calcium concentration act as a ubiquitous intracellular signal responsible for controlling a plethora of biological processes such as contraction, secretion, fertilization, cell proliferation, apoptosis, learning, and memory (*1*−*3*). In all eukaryotic cells, one of the key proteins that mediates Ca^{2+} signaling is calmodulin (CaM)[1] (*4*). Upon Ca^{2+} stimulation, CaM binds to and modulates the activity of a diverse number of enzymes, including a family of CaM-dependent serine/threonine protein kinases (*5*). CaM is a 148-amino acid protein whose crystal structure shows an extended dumbbell shape, with the N- and C-terminal domains connected by a solvent-exposed α-helix (*6*−*8*) that is flexible in solution (*9*, *10*). This flexibility is crucial for the binding and activation of target enzymes. The binding of Ca^{2+} to CaM induces conformational changes in its N- and C-domains, resulting in the exposure of hydrophobic pockets that are important for target protein binding (*11*−*13*).

The structural basis of the interaction of CaM with its target proteins has largely been investigated using synthetic peptides based on the binding domains of the intact target proteins. So far, CaM complexes with kinase enzymes have not been amenable to crystallization. Three-dimensional structures are available for CaM in complex with peptides derived from smMLCK (*14*), the plasma membrane Ca^{2+} pump (*15*), CaMKIIα (*16*), CaMKKα (*17*, *18*), and skMLCK (*19*). Target binding induces a large structural change in CaM whereby its N- and C-terminal domains wrap around the peptide. In general, the typical CaM-binding peptide is approximately 20 residues long and adopts an α-helical conformation in the complex. Two hydrophobic residues in this helix provide important anchor points for the interaction with the two CaM lobes (*20*). The N-terminal anchor residue of the target peptide is often a tryptophan residue (Figure 1A). More recently, the crystal structures of complexes with Oedema factor (a CaM-activated anthrax adenylyl cyclase) (*21*) and the gating domain of a Ca^{2+}-activated K^+ channel (*22*) have been determined. Altogether, these structures reveal the diverse ways in which target recognition and enzyme activation are performed by CaM (*23*).

‡ The coordinates for the complex between CaM and CaMKIp have been submitted to the Protein Data Bank (1MXE).

* To whom correspondence should be addressed. Telephone: +44-208-959-3666. Fax: +44-208-906-4477. E-mail: sgambli@nimr.mrc.ac.uk.

§ Division of Protein Structure.

|| These authors contributed equally to this work.

⊥ Division of Physical Biochemistry.

[1] Abbreviations: CaM, calmodulin; CaMKI, CamKII, and CaMKIV, CaM-dependent protein kinase I, II, and IV, respectively; CaMKIp, CaM-binding peptide of CaMKI (residues 294−318); CaMKK, CaM kinase kinase; skMLCK, skeletal muscle myosin light chain kinase; smMLCK, smooth muscle MLCK; NM2, Ac-ATKWQASFRGHITRK-KLKG-NH_2; WFF, KRRWKKNFIAVSAANRFK; FWF, KRRFKKN-WIAVSAANRFK; FFFu, KRRFKKNFIAVSAANRFK; FFFp, FFFu with N-terminal acetylation and C-terminal amidation; CBP1, LKLKKLL-KLLKKLLKLG; ADR1G, LKKLTRRASFSGQ; TCEP, tris(2-carboxyethyl)phosphine.

10.1021/bi026660t CCC: $22.00
Published on Web 11/19/2002

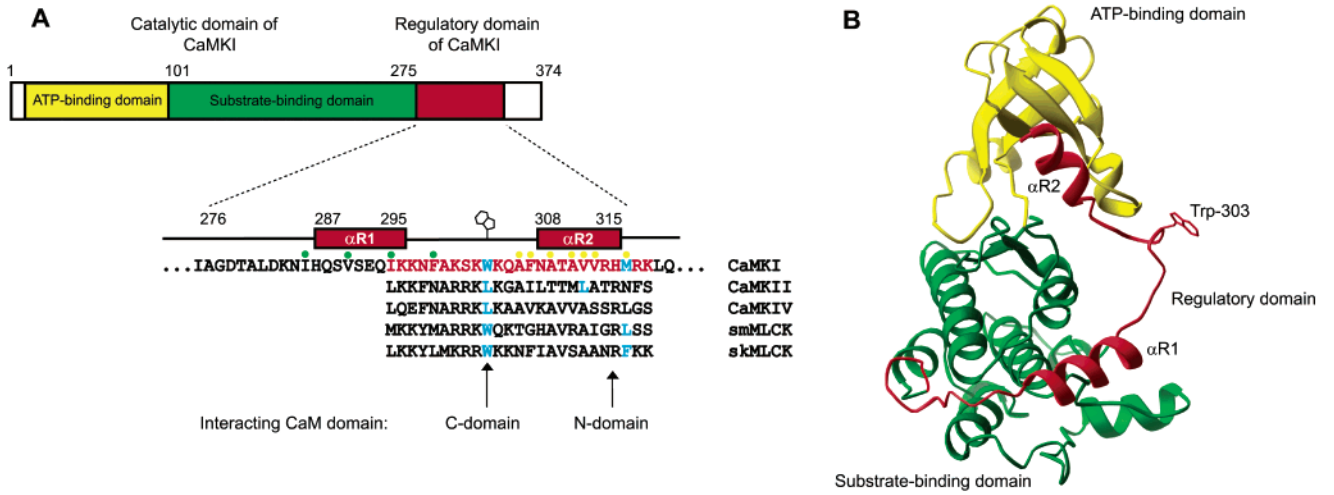

FIGURE 1: (A) Alignment of the CaM-binding sequences of rat CaMKIIα$^{(290-314)}$, rat CaMKIV$^{(313-337)}$, chicken smMLCK$^{(791-815)}$, and rabbit skMLCK$^{(571-595)}$ with rat CaMKI. The key hydrophobic residues for CaM binding are shown in blue. Green and yellow dots denote hydrophobic residues in the regulatory domain of CaMKI whose side chains pack against the substrate- and ATP-binding domains of autoinhibited CaMKI, respectively (*28*). (B) Structure of autoinhibited CaMKI$_{320}$ showing the orientation of the regulatory sequence with respect to the kinase ATP- and substrate-binding domains (PDB entry 1A06).

CaM-dependent protein kinase I (CaMKI) forms part of the CaM-dependent signaling cascade (*24*) together with CaMKIV and their upstream activator CaMK kinase (CaMKK). CaMKI is a widely distributed protein of 374 amino acids (*Rattus norvegicus*) that can phosphorylate several substrates, including the synaptic vesicle-associated proteins, synapsin 1 and 2 (*25*), and the cAMP response element-binding protein, CREB (*26*). The substrate recognition sequence for CaMKI is Hyd-X-Arg-X-X-Ser/Thr-X-X-X-Hyd, where Hyd is a hydrophobic residue at positions P−5 and P4 relative to the Ser/Thr residue at the phosphorylation site (*27*).

The crystal structure of a truncated form of the enzyme (residues 1−320) has been determined (*28*) and is shown in Figure 1B. The truncated enzyme (CaMKI$_{320}$) resembles the full-length form in being autoinhibited and displaying wild-type (wt) kinase activity when activated by CaM (*29*). The structure shows that the kinase is maintained in an autoinhibited state by the interaction of a regulatory sequence (residues 276−316) with the catalytic core of the enzyme (residues 10−275) (*28*). The regulatory sequence interacts with the catalytic domain of the kinase via two α-helices, αR1 and αR2, which are separated by a protruding loop. This regulatory segment contains a CaM-binding site, and it has been suggested that the solvent-exposed Trp-303, located on the loop, is involved in the initial CaM binding (*28*). Residues from helix αR1 and part of the protruding loop make contacts with the presumed substrate-binding channel of the kinase C-terminal lobe. Two such contacts involve Phe-298 and Lys-300 from the regulatory sequence, which appear to mimic the preferred hydrophobic P−5 and basic P−3 positions of the CaMKI substrate sequence. Residues from helix αR2 (Asn-308−His-315) and Met-316 make extensive hydrophobic interactions with the N-terminal ATP-binding domain, resulting in a distortion of the nucleotide-binding site. Therefore, the regulatory sequence of CaMKI$_{320}$ forms interactions with the catalytic domain that interfere with both substrate and ATP binding. Truncation at the C-terminus of the kinase to residue 293 (CaMKI$_{293}$) produces an enzyme that is constitutively active and CaM-independent (*29*, *30*). This observation, together with the crystal structure of autoinhibited CaMKI$_{320}$ (*28*), indicates that the pseudosubstrate segment and the CaM-binding sequence of CaMKI are located to the C-terminal side of Ile-293.

In this study, we have investigated the binding affinities and molecular interactions of CaM and its separate domains, with CaMKI$_{320}$ and a 25-residue peptide sequence containing the CaM-binding domain of CaMKI (CaMKIp, residues Ile-294$_{PEP}$−Lys-318$_{PEP}$) using crystallographic and spectroscopic techniques. The crystal structure of the complex, taken together with the spectroscopic and enzymatic data, reveals details of how both domains of CaM are involved in binding to the CaMKI target. We have characterized extensive electrostatic and hydrophobic contacts between CaM and the peptide, which allows a detailed analysis of the structural basis of the kinase activation process in terms of the overlap of the pseudosubstrate sequence and the CaM-binding sequence. CaM mutants involving the deletion of residues in the N-terminal sequence at positions 1−8 (*51*) are shown to activate the kinase, but with increased K_m values for ATP. This suggests the existence of additional interactions between the CaM N-domain and the core of the enzyme.

MATERIALS AND METHODS

Purification of Proteins and Peptides. Drosophila CaM was expressed in *Escherichia coli* and purified as described elsewhere (*31*). The tryptic fragments of CaM (CaM N-domain and CaM C-domain) were prepared as described by Barth et al. (*32*). The kinase peptide, CaMKIp [CaMKI$^{(294-318)}$, IKKNFAKSKWKQAFNATAVVRHMRK] was end-protected by N-terminal acetylation and C-terminal amidation, and was purchased from the University of Bristol (Bristol, U.K.). Peptide concentrations were determined spectrophotometrically using calculated ϵ_{278} values (*33*).

Preparation of SeMet CaM, CaMKI$_{320}$, CaMKI$_{293}$, and CaM N-Terminal Deletion Mutants. CaMKI$_{320}$ and CaMKI$_{293}$ were expressed as GST fusion proteins as described by Yokokura et al. (*29*). The plasmids that were used were gifts

Table 1: X-ray Data Collection, Phasing, and Refinement

Data Collection				
space group	$P2_12_12_1$			
cell parameters (Å)	SeMet, $a = 66.1$, $b = 69.4$, $c = 75.3$; native, $a = 65.7$, $b = 69.6$, $c = 75.3$			
	remote	edge	peak	native
wavelength (Å)	0.9500	0.9794	0.9791	0.9340
resolution (Å)	30.0−2.8	30.0−2.8	30.0−2.8	30.0−1.7
redundancy[a]	4.0	5.3	5.1	23.1
completeness (%)	83.8 (86.9)	98.9 (99.3)	99.1 (99.5)	99.9 (100.0)
R_{merge} (%)[b]	5.1 (6.7)	5.4 (6.8)	6.1 (7.1)	7.7 (21.7)
$I/\sigma(I)$	17.8 (15.3)	19.8 (19.7)	18.2 (18.7)	24.1 (7.0)

Phasing								
resolution bin (Å)	20.0−9.37	9.37−6.16	6.16−4.89	4.89−4.17	4.17−3.70	3.70−3.36	3.36−3.10	3.10−2.80
FOM	0.68	0.81	0.80	0.77	0.79	0.80	0.79	0.78
mean FOM	0.78							

Refinement					
resolution limits (Å)	30.0−1.70	no. of atoms		rms deviation	
R_{cryst} (%)[c]	18.8	protein	2682	bond lengths (Å)	0.010
R_{free} (%)[d]	22.8	Ca^{2+}	8	bond angles (deg)	1.205
		water	236		

[a] N_{obs}/N_{unique}. [b] $R_{merge} = \sum\sum_j|I_j - \langle I\rangle|/\sum\langle I\rangle$, where I_j is the intensity of the jth reflection and $\langle I\rangle$ is the average intensity. [c] $R_{cryst} = \sum_{hkl}|F_o - F_c|/\sum_{hkl}|F_o|$. [d] R_{free}, as for R_{cryst} but calculated on 5% of the data excluded from the refinement calculation.

from A. Nairn (Rockefeller University, New York, NY). The GST was removed by proteolytic cleavage with thrombin as described by Goldberg et al. (*28*). Selenomethionine (SeMet) CaM was prepared and purified as described by Yuan et al. (*34*). The N-terminal deletion mutants of CaM were a kind gift from A. Persechini (University of Missouri, Kansas City, MO).

Determination of Peptide Affinities. Dissociation constants were determined using either direct fluorometric titrations (*35*) or fluorometric competition assays (S. R. Martin and P. M. Bayley, *Protein Science*, in press). Measurements were taken at 20 °C in 25 mM Tris (pH 8.0) and 100 mM KCl, with 0.2 mM $CaCl_2$ or 0.2 mM EDTA as appropriate. Three independent titrations were performed, and the average value is reported with its standard deviation.

Kinase Activity Measurements. Kinase activity measurements using the ADR1G substrate peptide (*36*) were taken using a continuous spectrophotometric assay based on one described by Cook et al. (*37*). A typical assay contained the following components in a total volume of 1 mL in a 10 mm path length cuvette: 50 mM Hepes (pH 7.5), 1 mM $CaCl_2$, 10 mM $MgCl_2$, 1 mM DTT, 12 units of pig heart L-lactic dehydrogenase, 8 units of rabbit muscle pyruvate kinase, 1 mM phosphoenolpyruvate, 200 μM NADH, 2 mM ATP, 200 μM ADR1G, and 1 nM $CaMKI_{320}$. Reactions were initiated by the addition of CaM, and rates (at 30 °C) were obtained by recording absorbance changes at 340 nM.

Crystallization. Crystals of the CaM−CaMKIp complex were grown by the hanging drop method at 16 °C. Two microliters of protein complex (18 mg/mL) in 20 mM Tris (pH 7.8), 30 mM NaCl, and 1 mM $CaCl_2$ was mixed with 2 μL of a well solution [50 mM sodium cacodylate (pH 5.5), 5 mM $CaCl_2$, and 53−60% MPD]. Within 1 week, diamond-shaped crystals grew to a typical size of 0.4 mm × 0.4 mm × 0.3 mm. The SeMet CaM−CaMKIp crystals were prepared similarly except using Hepes buffer.

Data Collection. The SeMet CaM−CaMKIp complex was determined by multiwavelength anomalous diffraction (MAD). MAD data to 2.8 Å resolution were collected using EH4 on ID14 at ESRF. The Se edge wavelengths were selected from the fluorescence spectrum of the crystal (Table 1). A native-data set was collected to 1.7 Å resolution. All crystals were flash-cooled directly from their mother liquor. Data reduction, merging, and scaling were carried out with the HKL programs DENZO and SCALEPACK (*38*). Relevant crystallography statistics are summarized in Table 1.

Structure Determination, Model Building, and Refinement. The positions of 16 of the potential 18 selenium sites in the asymmetric unit were found with the program SOLVE (*39*). Experimental phases were improved by solvent flattening using RESOLVE (*40*) which produced readily interpretable electron density maps. The polypeptide chain of the model was built into the MAD electron density using the program O (*41*). The atomic model was refined against all of the native data, using REFMAC5 (*42*) interspersed with rounds of manual model building. Water molecules were built into the structure using ARP (*43*) with REFMAC5 (*42*).

RESULTS AND DISCUSSION

Structure Determination. The asymmetric unit contains two molecules of CaM each bound to a CaMKI peptide (final electron density for residues Lys-296_{PEP}−Val-312_{PEP} of CaMKIp shown in Figure 2). The final model contains 338 residues, 236 water molecules, and eight calcium ions, refined to an R_{cryst} of 18.8% and an R_{free} of 22.8% (Table 1). The root-mean-square deviation (rmsd) for the main chain atoms between the two molecules (A and B) in the asymmetric unit is 0.39 Å, and they have average B factors of 31.2 and 37.8 Å^2, respectively. The first three residues and last residue of CaM are not visible in the electron density maps. The quality of the model was assessed with PROCHECK (*44*). There are no Ramachandran outliers, and 95% of the molecule lies within the most favored region of the plot.

Overall Structure. The structure of the CaM−CaMKIp complex is shown in two orthogonal views in panels A and B of Figure 3. The most significant change in the overall CaM conformation upon binding to the peptide occurs in the interdomain linker region. In the complex with CaMKIp,

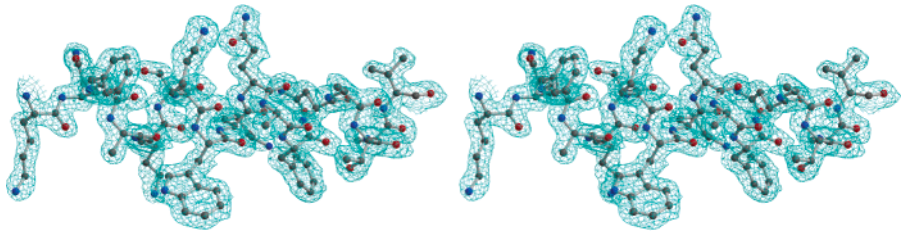

FIGURE 2: Stereoview of the final $2|F_o| - |F_c|$ electron density map, contoured at 1σ around residues Lys-296_{PEP}−Val-312_{PEP} of CaMKIp.

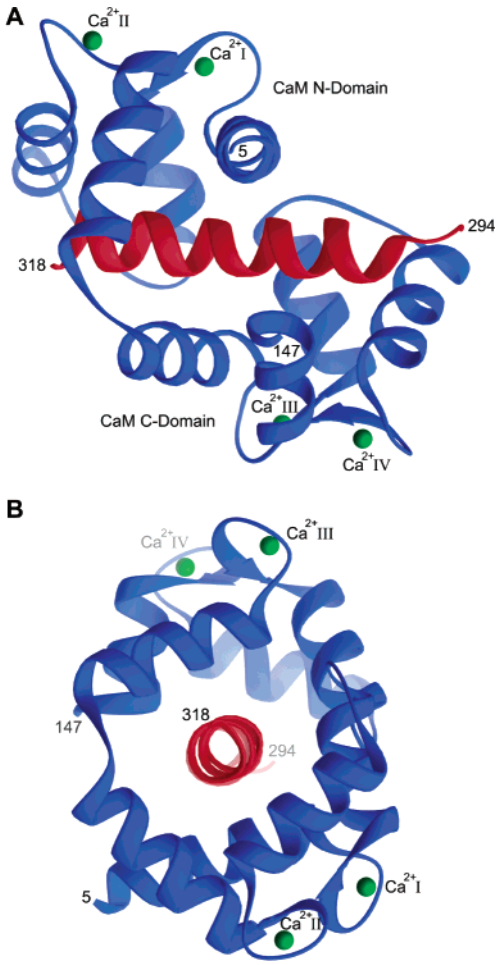

FIGURE 3: Ribbon drawings showing two orthogonal views of the CaM−CaMKIp complex. The peptide is highlighted in red, and calcium ions are drawn as green spheres. This figure was generated with RIBBONS (*53*). Residues Phe-298_{PEP}−Arg-317_{PEP} of the peptide adopt an α-helical conformation, whereas the first four residues and the last residue do not strictly conform to the Ramachandran angles required of an α-helix.

the linker is nonhelical from residue 79 to 80 and is bent by ~100° with respect to the crystal structure of non-peptide-bound CaM (*8*). The homologous N- and C-terminal domains of CaM come together and form a compact ellipsoidal structure with approximate dimensions of 50 Å × 35 Å × 35 Å. The close association of the hydrophobic faces of the two CaM lobes creates a central tunnel for accommodation of the peptide. Similar structural reorganization upon binding to target sequences has also been observed in the structures of CaM bound to peptides from skMLCK (*19*), smMLCK (*14*), CaMKIIα (*16*), and CaMKKα (*17*, *18*). The main chain conformations of N-domain residues 5−75 and C-domain residues 82−147 remain largely unchanged upon binding to CaMKIp. The rmsd values for the main chain atoms between free CaM (*8*) and the present structure are 0.71 and 0.75 Å for the N- and C-lobes, respectively. Recently, Kranz et al. (*45*) showed by NMR that the backbone conformation of CaM in a complex with a slightly shorter peptide from the CaM-binding sequence of CaMKI (residues 299−320) corresponds closely to the complex of CaM with the $CaMKI_{320}$ enzyme in solution.

In the complex of CaMKIp with CaM, the N-terminal region of the peptide primarily interacts with the C-domain of CaM, while the C-terminal sequence of the peptide primarily interacts with the CaM N-domain. This is a common feature of CaM−peptide structures, an exception being the case of CaMKKα where the direction of the peptide is reversed with respect to CaM (*17*, *18*). The peptide (Ile-294_{PEP}−Lys-318_{PEP}), which is unstructured in solution (data not shown), is completely ordered within the complex and adopts an α-helical conformation from residue Phe-298_{PEP} to Arg-317_{PEP}. It is interesting to note that residues Lys-296−Phe-307 are not helical in the structure of autoinhibited $CaMKI_{320}$ (*28*) but form a loop between αR1 and αR2 in the kinase regulatory region (Figure 1B). Moreover, the exposed Trp-303 and flanking residues appear to be stabilized by crystal lattice contacts. This region is proposed to be flexible in solution and available for initial interaction with CaM (*28*). Fluorescence emission properties (*46*) and this work (see below) are consistent with Trp-303 being solvent accessible.

Hydrophobic Binding Interface. Binding of CaM to CaMKIp buries nearly 60% of the peptide's solvent accessible area. The total area of the binding interface is 3340 Å^2, and extensive contacts, shown in Figure 4, account for the strong interaction between CaM and CaMKIp ($K_d \sim 1$ pM; see below). From the crystal structure of autoinhibited $CaMKI_{320}$ (*28*), the binding interface between equivalent residues in the regulatory sequence (Ile-294−Met-316) and the rest of the kinase is somewhat smaller, having a total buried surface area of 2040 Å^2. Hydrophobic interactions formed by the CaM and peptide side chains constitute a large proportion of the contacts; 74% of the total area of the binding interface is nonpolar.

The spacing and position of two bulky hydrophobic residues of the target sequence are important features in characterizing the modes of binding for CaM effector molecules (*20*); for example, in the peptide structure of CaMKIIα (*16*), Leu-299 and Leu-308 exhibit 1−10 spacing. In the structure reported here, Trp-303_{PEP} and Met-316_{PEP} show 1−14 spacing, analogous to that in the CaM−MLCKp complexes (*14*, *19*). These complexes also have similar global structures associated with the molecular recognition of their target peptides, and very similar polypeptide backbone conformations. For example, the rmsd between the CaM−CaMKIp and CaM−smMLCKp complexes for all Cα

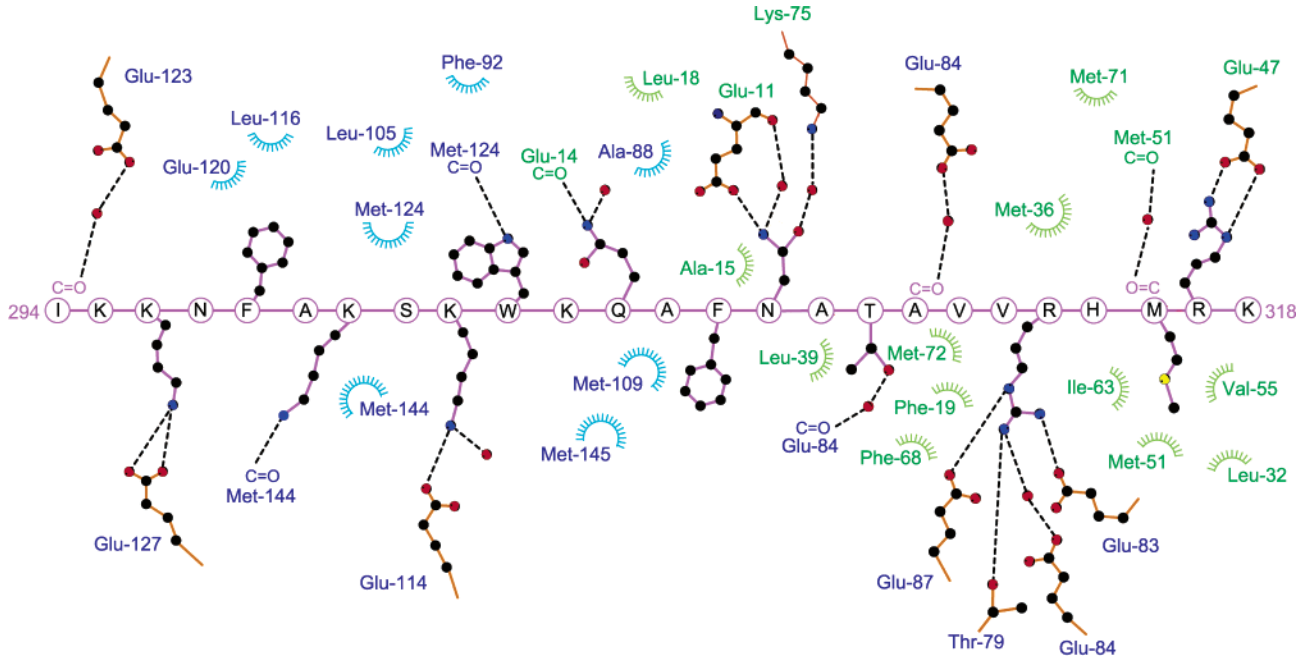

FIGURE 4: Schematic drawing showing the extensive interactions of the CaM N-domain (labeled green) and the CaM C-domain (blue) with CaMKIp. This figure was drawn with LIGPLOT (*54*). Peptide residues are drawn in purple, and the interacting CaM residues are colored brown.

atoms is 0.55 Å for the CaM N-domains and 0.96 Å for the CaM C-domains. When both domains are used in the superposition, the rmsd increases to 1.30 Å, showing that there is relatively little change in the relative orientations of the CaM domains between the two complexes.

Trp-303$_{PEP}$ interacts with numerous residues in the hydrophobic pocket of the CaM C-terminal lobe (Figure 5A) and can be regarded as an important "anchor" point in the CaM−CaMKIp complex. The side chains of Trp-303$_{PEP}$ and Met-124$_{CaM}$ form hydrophobic contacts with each other, and the carbonyl oxygen of Met-124$_{CaM}$ also forms a hydrogen bond with NE atom of the Trp indole ring. Additionally, the side chains of Met-144$_{CaM}$ and Met-145$_{CaM}$ make van der Waals interactions with the Trp-303$_{PEP}$ aromatic ring, and the side chain of Phe-92$_{CaM}$ switches its stacking partner from Phe-141 in free CaM (*8*) to interact with the side chain of Trp-303$_{PEP}$ in the complex. Site-directed mutagenesis studies involving the nine methionine residues of CaM also highlighted the role of some of these residues in complex formation with CaMKI (*36*). In particular, CaM Met-124$_{CaM}$ → Gln displays at least 60-fold weaker binding to CaMKI (*36*). The direct structural involvement of Met-124$_{CaM}$ is also provided by other CaM−peptide complexes (*14*, *16*).

In the structure presented here, the hydrophobic pocket of the CaM N-domain is occupied by the side chain of Met-316$_{PEP}$. Located toward the C-terminus of the target peptide, this Met makes hydrophobic interactions with the following N-terminal residues of CaM: Leu-32$_{CaM}$, Met-51$_{CaM}$, Val-55$_{CaM}$, Ile-63$_{CaM}$, and Met-71$_{CaM}$ (Figure 5B). A water-mediated hydrogen bond is also formed between the carbonyl oxygen atoms of Met-51$_{CaM}$ and Met-316$_{PEP}$. The role of Met-316 is particularly intriguing given the suggestion of its importance in maintaining the inactive form of the kinase (*28*). Together with residues Ala-306, Phe-307, Ala-309, Ala-311, Val-312, and Val-313, it forms part of the C-terminal portion of the regulatory sequence of CaMKI that interacts with the ATP-binding loop. In addition, the simultaneous substitution of N-domain residues that interact with Met-316$_{PEP}$ (Leu-32$_{CaM}$ → Ala, Met-51$_{CaM}$ → Ala, Val-55$_{CaM}$ → Ala, Phe-68$_{CaM}$ → Ala, and Met-71$_{CaM}$ → Ala) has been shown to increase the $K_{m,ATP}$ of CaMKI$_{433}$ 10-fold, but to have no effect on the K_m for the substrate peptide, ADR1G (*36*). Therefore, these N-terminal CaM substitutions specifically affect the ability of CaM to promote ATP binding in the nucleotide-binding site of the kinase.

Electrostatic Complementarity between CaM and CaMKIp. The electrostatic surface potential of CaM and CaMKIp is shown in Figure 6A and reveals the electrostatic complementarity between CaM and its target peptide. While the peptide is generally basic, and the CaM acidic, salt bridges between the two mainly occur at two specific sites (Figures 4 and 6B). Just prior to the N-terminal Trp-303$_{PEP}$ of CaMKIp, there is a cluster of four lysine residues (295, 296, 300, and 302). Two of these, Lys-296$_{PEP}$ and Lys-302$_{PEP}$, make electrostatic interactions with Glu-127$_{CaM}$ and Glu-114$_{CaM}$, respectively. The C-terminal region of CaMKIp has three basic residues (Arg-314$_{PEP}$, His-315$_{PEP}$, and Arg-317$_{PEP}$) that straddle Met-316$_{PEP}$. The side chain of Arg-314$_{PEP}$ forms three hydrogen bonds via its NH2, NH1, and NE atoms with the surrounding acidic residues Glu-83$_{CaM}$, Glu-84$_{CaM}$, and Glu-87$_{CaM}$, respectively. The interaction between Arg-314$_{PEP}$ and Glu-84$_{CaM}$ is mediated via a water molecule, and there is a salt bridge between Arg-317$_{PEP}$ and Glu-47$_{CaM}$.

Both hydrophobic and basic residues on the target peptide have been proposed to be important for determining the orientation with which CaM binds to its targets (*20*). For example, in structures of CaM bound to peptides from CaMKIIα (*16*) and smMLCK (*14*), electrostatic interactions are concentrated around the key N-terminal hydrophobic residues of these peptides. In the CaM−CaMKIp structure, electrostatic interactions are present around both hydrophobic anchors of the target peptide, yet the orientation of peptide binding is the same as that of the CaM−CaMKIIα and CaM−smMLCK peptide complexes. In contrast, in the

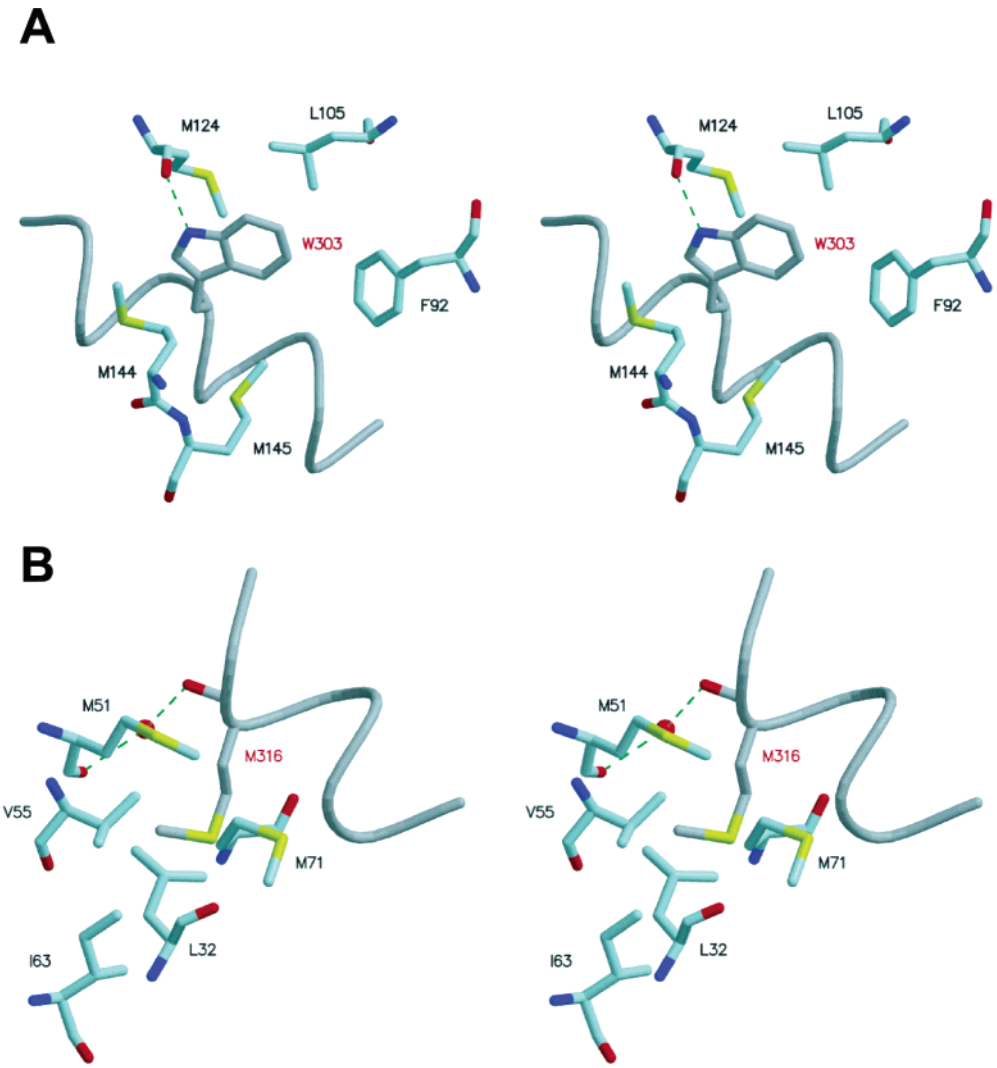

FIGURE 5: Stereodrawing of the key hydrophobic anchor residues of CaMKIp in the hydrophobic pocket of (A) the CaM C-domain and (B) the CaM N-domain. Only residues from CaM interacting with Trp-303$_{PEP}$ and Met-316$_{PEP}$ are shown. N, O, and S atoms are colored in blue, red, and yellow, respectively, while C atoms of CaM are shown in pale blue. A worm representation of the CaMKIp backbone is drawn in gray. This figure was generated with MOLSCRIPT (*55*) and Raster3D (*56*).

CaM−CaMKKα peptide complex (*17*, *18*), there is no basic cluster adjacent to the N-terminal tryptophan, but instead, there is a basic cluster near the conserved C-terminal hydrophobic anchoring residue. As a result, the CaMKKα peptide binds to CaM in a parallel fashion such that the N-terminal residues interact with the N-domain of CaM and the C-terminal residues interact with the CaM C-domain.

Determination of the Binding Affinity of CaM for CaMKIp and CaMKI$_{320}$. The binding of the peptide CaMKIp to CaM is characterized by an intense near-UV CD difference spectrum (Figure 7A) with pronounced positive ^1L_a and ^1L_b fine structural components at 293 and 286 nm, typical of an immobilized Trp residue (*47*), and by a marked blue shift of the Trp fluorescence emission (Figure 7B). Since the binding affinity of the isolated regulatory sequence of CaMKIp with CaM is very high, it was determined using a series of competition assays with peptides of increasingly high (lower than micromolar) affinity (see the Supporting Information). Figure 7C shows competition titrations of the CaM−CaMKIp complex with the peptides FFFu, FFFp, and CBP1. From these experiments, the K_d value for the affinity of CaMKIp with CaM is 0.3−1 pM. This is one of the highest affinities observed so far for such complexes, being greater than that of the skMLCK target peptide (*48*). This is consistent with the significant binding interface observed in our structure.

The near-UV CD spectrum of the kinase, CaMKI$_{320}$, shows intense negative bands deriving from the 14 Tyr and five Trp residues (Figure 8A); the difference spectrum generated upon binding CaM is characterized by a positive ^1L_a,^1L_b band shape similar to that of the CaM−CaMKIp complex (but ∼50% as intense). The fluorescence spectrum of CaMKI$_{320}$ (Figure 8B) contains contributions from all five Trp residues, of which three are clearly buried (*28*); the difference spectrum shows that CaM induces a blue shift similar to that observed with CaMKIp. The CD and fluorescence changes are consistent with CaM causing marked changes in the environment of Trp-303 in the kinase. Figure 8C shows the titration of the kinase with CaM, giving a K_d of 29 ± 6 nM. Similar results were obtained using labeled CaM (see the Supporting Information).

Thus, the peptide CaMKIp has an affinity for CaM that is ∼30000-fold greater than that of CaMKI$_{320}$. We deduce that binding of CaM to the intact enzyme necessitates expenditure of substantial free energy in the disruption of the interactions between the regulatory sequence and the enzyme core. The

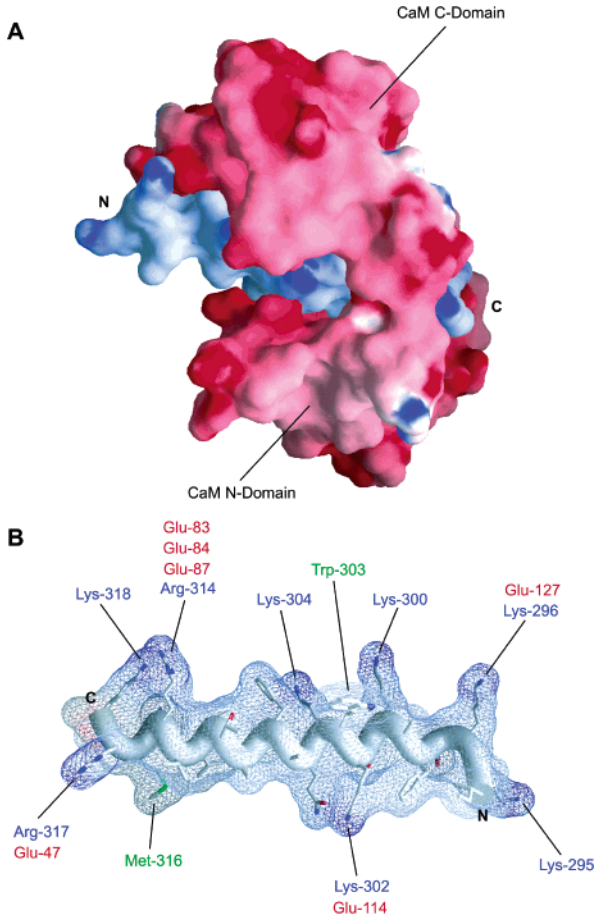

FIGURE 6: Electrostatic surface potential of the CaM−CaMKIp complex. In panel A, the molecular surfaces of CaM and CaMKIp are shown. The surface is colored according to the local electrostatic potential, with blue and red representing positive and negative potential, respectively. In panel B, a mesh representation of the electrostatic surface potential of CaMKIp is shown. The peptide backbone is drawn as a worm. Basic residues in the CaMKI peptide are labeled in blue and interacting acidic residues from CaM in red. The two main hydrophobic anchor points of the target peptide are labeled in green. This figure was generated with GRASP (*57*).

high affinity of the interaction of CaM with the regulatory sequence evidently partially compensates for the energetic requirements of the conformational change involved in the activation.

Domain Specificity of CaM for CaMKIp and CaMKI$_{320}$. To delineate the contributions of the two CaM domains in target binding, the interactions of the isolated N- and C-domains with CaMKIp and CaMKI$_{320}$ were studied by solution methods. Previous studies with individual domains showed that both domains could form 2:1 complexes (with differing affinities) with the skMLCK peptide (*32*). Tryptophan fluorescence titrations of CaMKIp with the CaM C-domain indicate formation of a 1:1 complex with a K_d of 6 ± 1.3 nM (Supporting Information). This result suggests that the isolated C-terminal domain of CaM interacts strongly and exclusively with the N-terminal portion of the regulatory peptide which contains Trp-303$_{PEP}$. The titrations of CaMKIp with the CaM N-domain showed more complex behavior (see the Supporting Information), but are consistent with two CaM N-domains binding to the peptide, with K_d values of 2.4 ± 0.7 and 1.1 ± 0.3 μM. Thus, the high affinity of the CaM C-domain for the Trp-303$_{PEP}$ region of the peptide appears to be the dominant determinant in CaM binding to

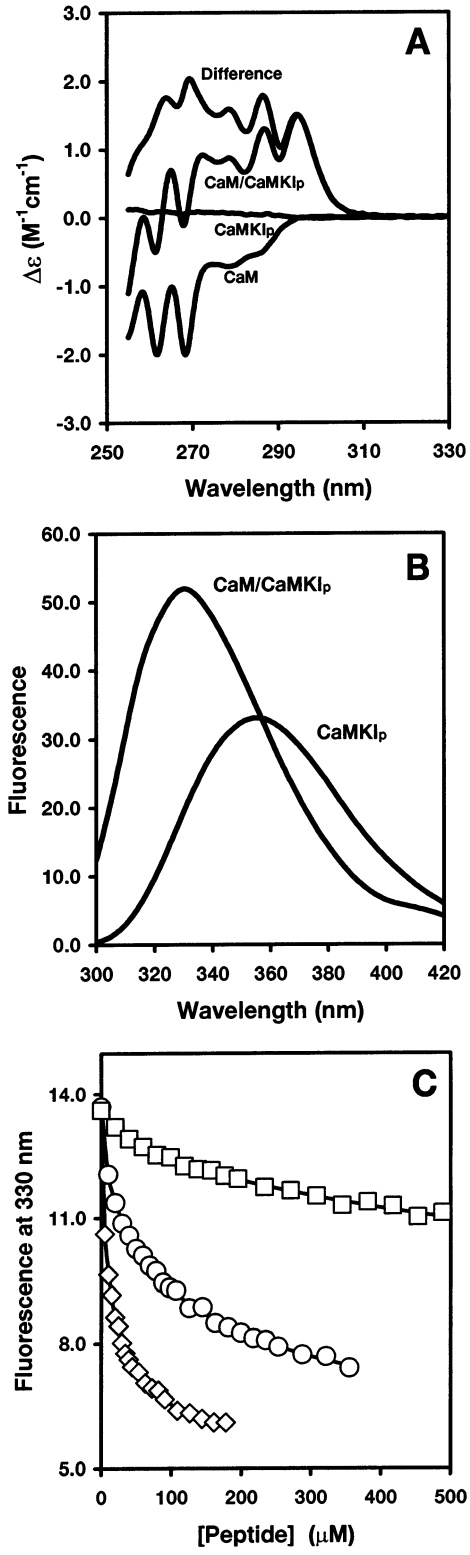

FIGURE 7: Interaction of CaM with CaMKIp. (A) Near-UV CD spectra of CaM, CaMKIp, and the CaM−CaMKIp complex. The difference spectrum was calculated as the complex minus components. (B) Fluorescence emission spectra of CaMKIp and the CaM−CaMKIp complex (excitation at 290 nm). (C) Titration of CaM (2 μM) and CaMKIp (2.1 μM) with peptides FFFu (□), FFFp (○), and CBP1 (◇). Solid lines are the computed best fits with values of K_d for CaMKIp of 1, 0.3, and 0.4 pM, respectively. Additional information is provided as Supporting Information.

CaMKI and, as with the target peptide of skMLCK (*32*), and with skMLCK, smMLCK, and NOS enzymes (*49*), determines the domain specificity of the peptide.

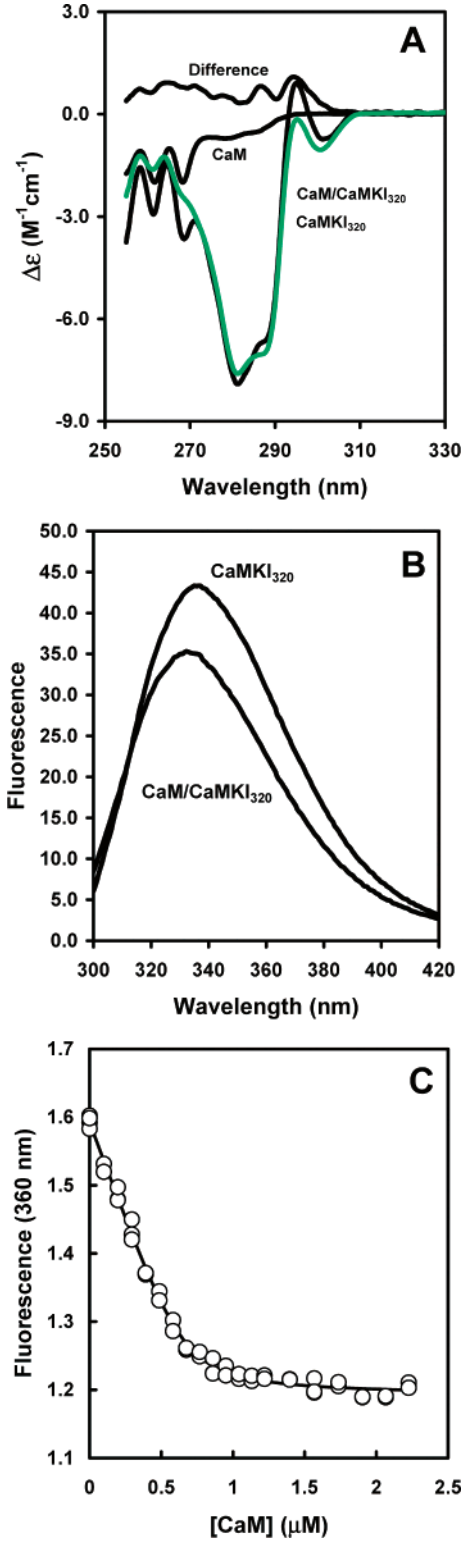

FIGURE 8: Interaction of CaM with $CaMKI_{320}$. (A) Near-UV CD spectra of CaM, $CaMKI_{320}$, and the CaM−$CaMKI_{320}$ complex. The difference spectrum was calculated as the complex minus components. The difference spectrum for CaM and CaMKIp is shown in Figure 7A. (B) Fluorescence emission spectra of $CaMKI_{320}$ and the CaM−$CaMKI_{320}$ complex (excitation at 290 nm). (C) Titration of $CaMKI_{320}$ (0.67 μM) with CaM.

Tryptophan fluorescence titrations of the intact kinase, $CaMKI_{320}$, with the CaM C-domain (data not shown) indicate formation of a 1:1 complex with a K_d of 1.4 ± 0.3 μM. As with the binding of full-length CaM, this value is significantly lower than that for binding to the peptide, CaMKIp. This implies that binding of the C-domain to $CaMKI_{320}$ does involve some disruption of interactions between the regulatory segment and the kinase, but this does not result in enzyme activation. In contrast, there was no evidence for an interaction between the intact kinase with the CaM N-domain. Neither of the isolated domains alone (up to 30 μM) was able to activate $CaMKI_{320}$, implying the obligatory requirement for concerted action by the two domains of the intact CaM molecule for production of enzyme activation. In contrast, skMLCK and other kinases have been shown to be activated by either individual domain, at a sufficiently high concentration (*49*).

Interactions of CaMKIp and ATP with Autoinhibited and Active Kinase. Direct binding of CaMKIp by CaM with high affinity means that CaMKIp is a strong inhibitor in the assay system for $CaMKI_{320}$. CaMKIp was found to inhibit the constitutively active truncated form of the kinase $CaMKI_{293}$ with ADR1G as the substrate (i.e., in the absence of CaM), with a K_I of approximately 2 μM (Supporting Information). Yokokura et al. (*29*) showed similar effects with a different substrate, syntide-2. These results show that CaMKIp can associate with the substrate-binding domain of (activated) $CaMKI_{293}$, inhibiting the binding of the substrate peptide. We have also compared the binding of ATP to $CaMKI_{293}$ and $CaMKI_{320}$. No direct interaction of ATP with $CaMKI_{320}$ could be detected using a range of spectroscopic parameters. Consistent with this, no effect on the directly determined affinity of CaM for $CaMKI_{320}$ was observed for ATP (up to 5 mM). Using the enzyme assay system, the $K_{m,ATP}$ for the truncated constitutively active enzyme, $CaMKI_{293}$, is 72 ± 14 μM, and for $CaMKI_{320}$ in the presence of CaM, it is 112 ± 15 μM (cf. ref *36*). Thus, ATP binding to $CaMKI_{320}$ is dependent on the presence of CaM, but occurs with a lower affinity than with $CaMKI_{293}$, suggesting some residual, or possibly novel, secondary interaction of the bound CaM with the nucleotide-binding site. These results show that the ATP site is functional only after activation by CaM, or after truncation of the autoinhibited enzyme.

Relationship of Autoinhibitory and CaM-Binding Sequences. Together with the crystal structure presented here and other structural and functional studies on CaMKI, it is now possible to accurately define the extent of overlap between the pseudosubstrate and the CaM-binding sequence of CaMKI. The structure of autoinhibited $CaMKI_{320}$ (*28*) reveals a series of hydrophobic interactions between residues Ile-286, Val-290, Ile-294, and Phe-298 of the regulatory domain and the presumed substrate-binding site of the kinase. These hydrophobic interactions were proposed to form the basis of inhibition of substrate binding; in particular, Phe-298 is thought to mimic the preferred hydrophobic residue at position P−5 in the substrate recognition sequence of CaMKI (*28*). This idea was largely supported by analysis of alanine substitutions at these four positions (*50*). In addition, measurements on the catalytic activity of C-terminally truncated CaMKI support this model and suggest a substantial role for Phe-298 and perhaps a lesser additional role for Lys-295 and Lys-296 (*50*). In our structure, residues $Lys\text{-}296_{PEP}$ and $Phe\text{-}298_{PEP}$ engage in interactions with CaM (Figure 4) and must therefore be regarded as part of the CaM-binding domain of CaMKI. It is interesting to note that both skMLCK and smMLCK contain bulky hydrophobic residues

Table 2: Kinetic Constants for Mutant $_{\Delta N}$CaM Activation of $CaMKI_{320}$

	wild type	$_{\Delta 2-4}$CaM	$_{\Delta 4-6}$CaM	$_{\Delta 6-8}$CaM	$_{\Delta 2-8}$CaM
K_{CaM} (nM)	4.5 (0.6)[a]	5.5 (0.8)	4.9 (0.5)	6.1 (0.7)	5.5 (0.8)
$K_{m,ADR1G}$ (μM)	7.1 (0.6)	7.8 (1.2)	8.1 (1.3)	6.5 (0.8)	7.1 (0.7)
$K_{m,ATP}$ (μM)	112 (15)	120 (15)	135 (15)	750 (120)	1400 (250)
relative V_{max}	100	95	105	80	55

[a] Values in parentheses are errors associated with the measurements.

at positions equivalent to Phe-298 in CaMKI. However, in these two cases, such residues have not been considered as part of the CaM-binding sequence.

The N-Terminal Sequence of CaM Is Important for CaMKI Activation. Persechini et al. (*51*) showed that deletions in the N-terminal leader sequence of CaM (Ala-1_{CaM}−Glu-8_{CaM}) affect the CaM-dependent activation of various kinases, including skMLCK. Consistent with crystal structures of several other CaM−peptide complexes, the structure presented here indicates no involvement of these CaM residues in direct interactions with the target peptide. We have, therefore, examined the activation of $CaMKI_{320}$ using four CaM N-terminal deletion mutants. Table 2 shows that $_{\Delta 2-4}$CaM and $_{\Delta 4-6}$CaM behave essentially as wild-type (wt) CaM. In contrast, $_{\Delta 6-8}$CaM and $_{\Delta 2-8}$CaM are clearly effective as activators, but exhibit a lower level of maximal activation than wt-CaM. They increase the K_m for ATP by at least 6- and 12-fold, respectively, but without altering substrate or CaM binding by the kinase. Thus, consistent with previous results (*51*), deletions involving the acidic cluster of Glu-6_{CaM}, Glu-7_{CaM}, and Gln-8_{CaM} affect the activation of $CaMKI_{320}$, but in a way different from that of skMLCK. Since the K_m for the substrate peptide remains unchanged, it suggests that $_{\Delta 2-8}$CaM retains the ability to relieve autoinhibition in the substrate−peptide binding area of the kinase. Possible effects on the $K_{m,ATP}$ with the other kinases were not previously reported (*51*), which may explain their apparently complete lack of activity in the presence of truncated CaM.

General Discussion. CaM-dependent activation of CaMKI is a complex process, which is not yet fully understood at the structural level. The current study has allowed us to analyze the relationship between the N- and C-terminal domains of CaM in this process. The combined requirement for both domains in kinase activation is evident. Consistent with the high-affinity complex formed between CaM and the CaMKI target peptide, our structure reveals multiple interactions between both domains of CaM and the peptide. Also, the importance of the CaM N-domain in relieving autoinhibition at the ATP-binding site of CaMKI and the C-domain at the substrate-binding site is strongly supported by the data presented here. The structure provides direct evidence for the overlap of the pseudosubstrate sequence and the CaM-binding sequence; the latter is seen to involve the key residue Phe-298_{PEP}, and appears to begin as early as residue Lys-296_{PEP}. The precise border between the two sequences has previously been hard to define using the functional criterion of progressive C-terminal truncation to eliminate first binding of CaM and subsequently the relief of autoinhibition. These findings have clear implications for the regulation of other autoinhibited systems via the binding of an external activator. A striking feature of the CaM−CaMKIp complex is that residues Phe-298_{PEP}−Arg-317_{PEP} of the peptide adopt a continuous α-helix conformation. This suggests that the activation mechanism probably involves the formation of such a helix, principally due to the change in the conformation of residues comprising the exposed, nonhelical sequence, seen as a loop in the crystal structure of autoinhibited CaMKI (*28*). The resulting complex between CaM and this segment of the kinase ultimately relieves autoinhibition of CaMKI. For example, the direct interaction of CaM with residues Lys-296 and Phe-298 of the kinase is required to generate a functional substrate-binding site, and the binding of CaM to residues in the αR2 region of the kinase allows relaxation of the nucleotide-binding domain and formation of a functional ATP site.

However, our analysis of the effect of $_{\Delta 2-8}$CaM on CaMKI activation suggests that there must be an additional role for the CaM N-domain beyond that just described. Removal of this short acidic segment from the N-terminus results in modulation of the properties of the ATP-binding site of CaMKI. The fact that N-terminal residues 6−8 do not interact with CaMKIp in our structure strongly suggests that they mediate secondary interactions, with as yet unidentified parts of the kinase distinct from the regulatory segment. In this light, it seems particularly intriguing that small-angle X-ray scattering experiments (*52*) have revealed a substantial change in the position of CaM relative to its target skMLCK, upon removal of these N-terminal CaM residues. Whereas full-length CaM was shown to occupy a position away from the catalytic core of the kinase, N-terminally truncated CaM was located near the active site of skMLCK, preventing enzyme activation. However, there is a marked difference in the activation levels of CaMKI and skMLCK observed with the N-terminally deleted CaM: $_{\Delta 2-8}$CaM completely abolishes CaM-dependent activation of skMLCK (*51*); in contrast, with $CaMKI_{320}$ it activates the kinase to ∼50% of the maximum level of activation found with wt-CaM. Thus, the precise details of the activation mechanism may be different for the two enzymes. Clearly, clarification of this issue will require the detailed structures of CaM in complex with both of the intact kinases, which until now have not been amenable to crystallization.

ACKNOWLEDGMENT

We thank Dr. Angus Nairn and Dr. Anthony Persechini for gifts of CaMKI constructs and CaM mutants, respectively, and Pete Browne for the expression and purification of cysteine mutants of CaM. We are grateful to our colleague Dr. Phil Walker for assistance.

SUPPORTING INFORMATION AVAILABLE

Details of the determination of dissociation constants for the interaction of CaMKIp and $CaMKI_{320}$ with CaM and its N- and C-terminal tryptic fragments, as well as the inhibition of $CaMKI_{293}$ by CaMKIp. This material is available free of charge via the Internet at http://pubs.acs.org.

REFERENCES

1. Carafoli, E. (2002) Calcium signaling: a tale for all seasons, *Proc. Natl. Acad. Sci. U.S.A. 99*, 1115−1122.
2. Berridge, M. J., Lipp, P., and Bootman, M. D. (2000) The versatility and universality of calcium signaling, *Nat. Rev. Mol. Cell Biol. 1*, 11−21.

3. Berridge, M. J., Bootman, M. D., and Lipp, P. (1998) Calcium-a life and death signal, *Nature 395*, 645−648.
4. Chin, D., and Means, A. R. (2000) Calmodulin: a prototypical calcium sensor, *Trends Cell Biol. 10*, 322−328.
5. Soderling, T. R., and Stull, J. T. (2001) Structure and regulation of calcium/calmodulin-dependent protein kinases, *Chem. Rev. 101*, 2341−2352.
6. Babu, Y. S., Bugg, C. E., and Cook, W. J. (1988) Structure of calmodulin refined at 2.2 Å resolution, *J. Mol. Biol. 204*, 191−204.
7. Babu, Y. S., Sack, J. S., Greenhough, T. J., Bugg, C. E., Means, A. R., and Cook, W. J. (1985) Three-dimensional structure of calmodulin, *Nature 315*, 37−40.
8. Chattopadhyaya, R., Meador, W. E., Means, A. R., and Quiocho, F. A. (1992) Calmodulin structure refined at 1.7 Å resolution, *J. Mol. Biol. 228*, 1177−1192.
9. Barbato, G., Ikura, M., Kay, L. E., Pastor, R. W., and Bax, A. (1992) Backbone dynamics of calmodulin studied by ^{15}N relaxation using inverse detected two-dimensional NMR spectroscopy: the central helix is flexible, *Biochemistry 31*, 5269−5278.
10. Heidorn, D. B., and Trewhella, J. (1988) Comparison of the crystal and solution structures of calmodulin and troponin C, *Biochemistry 27*, 909−915.
11. Kuboniwa, H., Tjandra, N., Grzesiek, S., Ren, H., Klee, C. B., and Bax, A. (1995) Solution structure of calcium-free calmodulin, *Nat. Struct. Biol. 2*, 768−776.
12. Finn, B. E., Evenas, J., Drakenberg, T., Waltho, J. P., Thulin, E., and Forsen, S. (1995) Calcium-induced structural changes and domain autonomy in calmodulin, *Nat. Struct. Biol. 2*, 777−783.
13. Zhang, M., Tanaka, T., and Ikura, M. (1995) Calcium-induced conformational transition revealed by the solution structure of apo calmodulin, *Nat. Struct. Biol. 2*, 758−767.
14. Meador, W. E., Means, A. R., and Quiocho, F. A. (1992) Target enzyme recognition by calmodulin: 2.4 Å structure of a calmodulin-peptide complex, *Science 257*, 1251−1255.
15. Elshorst, B., Hennig, M., Forsterling, H., Diener, A., Maurer, M., Schulte, P., Schwalbe, H., Griesinger, C., Krebs, J., Schmid, H., Vorherr, T., and Carafoli, E. (1999) NMR solution structure of a complex of calmodulin with a binding peptide of the Ca^{2+} pump, *Biochemistry 38*, 12320−12332.
16. Meador, W. E., Means, A. R., and Quiocho, F. A. (1993) Modulation of calmodulin plasticity in molecular recognition on the basis of X-ray structures, *Science 262*, 1718−1721.
17. Osawa, M., Tokumitsu, H., Swindells, M. B., Kurihara, H., Orita, M., Shibanuma, T., Furuya, T., and Ikura, M. (1999) A novel target recognition revealed by calmodulin in complex with Ca^{2+}-calmodulin-dependent kinase kinase, *Nat. Struct. Biol. 6*, 819−824.
18. Kurokawa, H., Osawa, M., Kurihara, H., Katayama, N., Tokumitsu, H., Swindells, M. B., Kainosho, M., and Ikura, M. (2001) Target-induced conformational adaptation of calmodulin revealed by the crystal structure of a complex with nematode Ca(2+)/calmodulin-dependent kinase kinase peptide, *J. Mol. Biol. 312*, 59−68.
19. Ikura, M., Clore, G. M., Gronenborn, A. M., Zhu, G., Klee, C. B., and Bax, A. (1992) Solution structure of a calmodulin-target peptide complex by multidimensional NMR, *Science 256*, 632−638.
20. Rhoads, A. R., and Friedberg, F. (1997) Sequence motifs for calmodulin recognition, *FASEB J. 11*, 331−340.
21. Drum, C. L., Yan, S. Z., Bard, J., Shen, Y. Q., Lu, D., Soelaiman, S., Grabarek, Z., Bohm, A., and Tang, W. J. (2002) Structural basis for the activation of anthrax adenylyl cyclase exotoxin by calmodulin, *Nature 415*, 396−402.
22. Schumacher, M. A., Rivard, A. F., Bachinger, H. P., and Adelman, J. P. (2001) Structure of the gating domain of a Ca^{2+}-activated K^+ channel complexed with Ca^{2+}/calmodulin, *Nature 410*, 1120−1124.
23. Hoeflich, K. P., and Ikura, M. (2002) Calmodulin in action: diversity in target recognition and activation mechanisms, *Cell 108*, 739−742.
24. Soderling, T. R. (1999) The Ca^{2+}-calmodulin-dependent protein kinase cascade, *Trends Biochem. Sci. 24*, 232−236.
25. Nairn, A. C., and Greengard, P. (1987) Purification and characterization of Ca^{2+}/calmodulin-dependent protein kinase I from bovine brain, *J. Biol. Chem. 262*, 7273−7281.
26. Sheng, M., Thompson, M. A., and Greenberg, M. E. (1991) CREB: a Ca^{2+}-regulated transcription factor phosphorylated by calmodulin-dependent kinases, *Science 252*, 1427−1430.
27. Lee, J. C., Kwon, Y. G., Lawrence, D. S., and Edelman, A. M. (1994) A requirement of hydrophobic and basic amino acid residues for substrate recognition by Ca^{2+}/calmodulin-dependent protein kinase Ia, *Proc. Natl. Acad. Sci. U.S.A. 91*, 6413−6417.
28. Goldberg, J., Nairn, A. C., and Kuriyan, J. (1996) Structural basis for the autoinhibition of calcium/calmodulin-dependent protein kinase I, *Cell 84*, 875−887.
29. Yokokura, H., Picciotto, M. R., Nairn, A. C., and Hidaka, H. (1995) The regulatory region of calcium/calmodulin-dependent protein kinase I contains closely associated autoinhibitory and calmodulin-binding domains, *J. Biol. Chem. 270*, 23851−23859.
30. Haribabu, B., Hook, S. S., Selbert, M. A., Goldstein, E. G., Tomhave, E. D., Edelman, A. M., Snyderman, R., and Means, A. R. (1995) Human calcium-calmodulin dependent protein kinase I: cDNA cloning, domain structure and activation by phosphorylation at threonine-177 by calcium-calmodulin dependent protein kinase I kinase, *EMBO J. 14*, 3679−3686.
31. Browne, J. P., Strom, M., Martin, S. R., and Bayley, P. M. (1997) The role of β-sheet interactions in domain stability, folding, and target recognition reactions of calmodulin, *Biochemistry 36*, 9550−9561.
32. Barth, A., Martin, S. R., and Bayley, P. M. (1998) Specificity and symmetry in the interaction of calmodulin domains with the skeletal muscle myosin light chain kinase target sequence, *J. Biol. Chem. 273*, 2174−2183.
33. Pace, C. N., Vajdos, F., Fee, L., Grimsley, G., and Gray, T. (1995) How to measure and predict the molar absorption coefficient of a protein, *Protein Sci. 4*, 2411−2423.
34. Yuan, T., Weljie, A. M., and Vogel, H. J. (1998) Tryptophan fluorescence quenching by methionine and selenomethionine residues of calmodulin: orientation of peptide and protein binding, *Biochemistry 37*, 3187−3195.
35. Findlay, W. A., Martin, S. R., Beckingham, K., and Bayley, P. M. (1995) Recovery of native structure by calcium binding site mutants of calmodulin upon binding of sk-MLCK target peptides, *Biochemistry 34*, 2087−2094.
36. Chin, D., Winkler, K. E., and Means, A. R. (1997) Characterization of substrate phosphorylation and use of calmodulin mutants to address implications from the enzyme crystal structure of calmodulin-dependent protein kinase I, *J. Biol. Chem. 272*, 31235−31240.
37. Cook, P. F., Neville, M. E., Jr., Vrana, K. E., Hartl, F. T., and Roskoski, R., Jr. (1982) Adenosine cyclic 3′,5′-monophosphate dependent protein kinase: kinetic mechanism for the bovine skeletal muscle catalytic subunit, *Biochemistry 21*, 5794−5799.
38. Otwinowski, Z., and Minor, W. (1997) Processing of X-ray diffraction data in oscillation mode, *Methods Enzymol. 276*, 307−326.
39. Terwilliger, T. C., and Berendzen, J. (1999) Automated MAD and MIR structure solution, *Acta Crystallogr. D55*, 849−861.
40. Terwilliger, T. C. (2000) Maximum-likelihood density modification, *Acta Crystallogr. D56*, 965−972.
41. Jones, T. A., Zou, J. Y., Cowan, S. W., and Kjeldgaard, M. (1991) Improved methods for building protein models in electron density maps and the location of errors in these models, *Acta Crystallogr. A47*, 110−119.
42. Murshudov, G. N., Vagin, A. A., and Dodson, E. J. (1997) Refinement of macromolecular structures by the maximum-likelihood method, *Acta Crystallogr. D53*, 240−255.
43. Perrakis, A., Morris, R., and Lamzin, V. S. (1999) Automated protein model building combined with iterative structure refinement, *Nat. Struct. Biol. 6*, 458−463.
44. Laskowski, R. A., MacArthur, M. W., Moss, D. S., and Thornton, J. M. (1993) PROCHECK: A program to check the stereochemical quality of protein structures, *J. Appl. Crystallogr. 26*, 283−291.
45. Kranz, J. K., Lee, E. K., Nairn, A. C., and Wand, A. J. (2002) A direct test of the reductionist approach to structural studies of calmodulin activity: relevance of peptide models of target proteins, *J. Biol. Chem. 277*, 16351−16354.
46. Gomes, A. V., Barnes, J. A., and Vogel, H. J. (2000) Spectroscopic characterization of the interaction between calmodulin-dependent protein kinase I and calmodulin, *Arch. Biochem. Biophys. 379*, 28−36.
47. Barth, A., Martin, S. R., and Bayley, P. M. (1998) Resolution of Trp near UV CD spectra of calmodulin-domain peptide complexes into the 1La and 1Lb component spectra, *Biopolymers 45*, 493−501.

48. Brown, S. E., Martin, S. R., and Bayley, P. M. (1997) Kinetic control of the dissociation pathway of calmodulin-peptide complexes, *J. Biol. Chem. 272*, 3389−3397.
49. Persechini, A., McMillan, K., and Leakey, P. (1994) Activation of myosin light chain kinase and nitric oxide synthase activities by calmodulin fragments, *J. Biol. Chem. 269*, 16148−16154.
50. Matsushita, M., and Nairn, A. C. (1998) Characterization of the mechanism of regulation of Ca^{2+}/calmodulin-dependent protein kinase I by calmodulin and by Ca^{2+}/calmodulin-dependent protein kinase kinase, *J. Biol. Chem. 273*, 21473−21481.
51. Persechini, A., Gansz, K. J., and Paresi, R. J. (1996) A role in enzyme activation for the N-terminal leader sequence in calmodulin, *J. Biol. Chem. 271*, 19279−19282.
52. Krueger, J. K., Gallagher, S. C., Zhi, G., Geguchadze, R., Persechini, A., Stull, J. T., and Trewhella, J. (2001) Activation of myosin light chain kinase requires translocation of bound calmodulin, *J. Biol. Chem. 276*, 4535−4538.
53. Carson, M. (1991) RIBBONS 2.0, *J. Appl. Crystallogr. 24*, 958−961.
54. Wallace, A. C., Laskowski, R. A., and Thornton, J. M. (1995) LIGPLOT: a program to generate schematic diagrams of protein−ligand interactions, *Protein Eng. 8*, 127−134.
55. Kraulis, P. J. (1991) MOLSCRIPT: A program to produce both detailed and schematic plots of protein structures, *J. Appl. Crystallogr. 24*, 946−950.
56. Merritt, E. A., and Murphy, M. E. P. (1994) Raster3D Version 2.0. A program for photorealistic molecular graphics, *Acta Crystallogr. D50*, 869−873.
57. Nicholls, A., Bharadwaj, R., and Honig, B. (1993) GRASP: graphical representation and analysis of surface properties, *Biophys. J. 64*, 166−170.

BI026660T